International Design Study for the Neutrino Factory

First progress report

Abstract

Some text for the abstract to go here.

The IDS-NF collaboration

27th January 2010

B. Reinhold
RWTH Aachen, Templergraben 55, 52062 Aachen, Germany

S.K. Argawalla, S. Choubey, R. Gandhi, S. Goswami
Harish-Chandra Research Institute, Chhatnag Road, Jhunsi, Allahabad, 211019, India

M. Guler
Middle East Technical Univ., Dept. of Physics, TR-06531 Ankara, Turkey

D. Perret-Gallix
LAPP - 9 Chemin de Bellevue - BP 110 F-74941, Annecy-le-Vieux CEDEX, France

E. Radicioni
Istituto Nazionale di Fisica Nucleare, via Amendola 173, I-70126 Bari, Italu

F. Sanchez
Institut de Fsica d'Altes Energies (IFAE), Edifici Cn, Universitat Autnoma de Barcelona (UAB), E-08193 Bellaterra (Barcelona), Spain

M. Messina
University of Bern, Laboratory for High Energy Physics, Sidlerstr. 5, CH-3012 Bern, Switzerland

T. Rovelli, M. Selvi
Istituto Nazionale Fisica Nucleare, Universita' di Bologna, V.le Berti Pichat, 6/2, Via Irnerio, 46, I-40126 Bologna, Italy

B.L. Roberts, L.R. Sulak
Boston University, Department of Physics, 590 Commonwealth Avenue, Boston, MA 02215, USA

S. Berg, S. Dawson, R. Fernow, J. Gallardo, S. Kahn, H. Kirk, H. Park, R. Palmer, N. Simos
Brookhaven National Lab, P.O. Box 5000, Upton, NY 11973-5000, USA

M. Ellis, P. Kyberd
Brunel Universiry West London, Uxbridge, Middlesex UB8 3PH, UK

J. Bouchez, C. Cavata
DAPNIA, CEA Saclay, Service de Physique des Particules, F-91191 Gif-sur-Yvette, CEDEX, FRANCE

M. Aiba, E. Benedetto, L. Camilleri, I. Efthymiopoulos, A. Fabich, F. Gerigk, R. Garoby, K. Hanke, E. Gschwendtner, C. Joram, E. Jeil, Y. Kadi, J. Lettry, G. Prior, C. Rossi, H. Schonauer, H. P. Sievers, G. Valenti, M. Vretenar
European Organization for Nuclear Research, CERN CH-1211, Geneva 23, Switzerland

K. Zuber
TU Dresden, Institut fuer Kern- und Teilchenphysik, D-01069 Dresden, GERMANY

M. Felcini
University College, National University of Ireland (Dublin), Dept. of Experimental Physics, Science Buildings, Belfield, Dublin 4, Ireland

B. Popov
Joint Institute for Nuclear Research, Joliot-Curie 6, 141980, Dubna, Moscow Region, RUSSIA

T. Li, S. Pascoli
Ogden Centre for Fundamental Physics, Department of Physics, University of Durham, Science Laboratories, South Rd, Durham, DH1 3LE, UK

C. Walter
Duke University, Department of Physics, Durham, NC 27706, USA

V. Bhatnagar, A. Bross, B. Choudhary, D. Finley, S. Geer, D. Harris, C. Johnstone, P. Lucas, J. Morfin, J. Nelson, D. Neuffer, K. Paul, A. Pla, A. Poklonskiy, M. Popovic, P. Rapidis, J. Strait, C. Yoshikawa, R. Zwaska
Fermilab, P.O. Box 500, Batavia, IL 60510-5011, US

A. Blondel, J.S. Graulich, R. Sandstrom
University de Geneve, 24, Quai Ernest-Ansermet, 1211 Geneva 4, Suisse

A. Laing, P. Soler, K. Walaron
Department of Physics and Astronomy, Kelvin Building, University of Glasgow, Glasgow G12 8QQ, Scotland, UK

L.S. Esposito, G. de Lellis
Istituto Nazionale di Fisica Nucleare, Laboratorio Nazionale del Gran Sasso, Strada Statale 17/bis Km 18+910, I-67010 Assergi (L'Aquila), Italy

A. Bueno
Universidad de Granada, DFTC, Dept. de Fisica Teorica y del Cosmos, Campus de Fuente Nueva, E-18002, Granada, SPAIN

F. Meot
Laboratory for Subatomic Physics and Cosmology (LPSC), Universite Joseph Fourier (Grenoble 1), 53, ave. des Marthyrs, F-38026 Grenoble CEDEX, France

J. Kopp, M. Lindner, T. Schwetz
Max-Planck-Institut fr Kernphysik, PO Box 103980, 69029 Heidelberg, Germany

T. Enqvist, P. Kuusiniemi, J. Peltoniemi
Univ. of Helsinki, Department of Physical Sciences, P.O. Box 64 (Vaino Auerin katu 11), FIN-00014, Helsinki, Finland

D. Kaplan, Y. Torun
Illinois Institute of Technology, 3300 South Federal Street, Chicago, IL 60616-3793, US

A. Alekou, M. Apollonio, C. Bontoiu, A. Dobbs, P. Dornan, A. Fish, A. Kurup, K. Long, J. Pasternak, J. Pozimski, Y. Uchida, D. Wark
Physics Deptartment, Blackett Laboratory, Imperial College London, Exhibition Road, London, SW7 2AZ, UK

D. Casper, H. Sobel
University of California, Dept. of Physics and Astronomy, High Energy Group, 4129 Frederick Reines Hall, Irvine, CA 92697-4575, USA

A. Bogacz
Jefferson Laboratory, 12000 Jefferson Avenue, Newport News, VA 23606, US

K. Nakamura, M. Sakuda, H. Sugiyama, K. Yoshimura
High Energy Accelerator Research Organization (KEK), Institute of Particle and Nuclear Studies, Tsukuba, Ibaraki, Japan

S. Bhattacharya, D. Majumdar
Saha Inst. Nuclear Phys., Sector-I, Block-AF, bidhannagar, Kolkata 700064, India

T. Nakaya
Kyoto Univ., Dept. of Physics, Kitashirakawa-Oiwakecho. Sakyo-ku, Kyoto 606-8502, Japan

Y. Mori
Kyoto University, Research Reactor Institute, 2,Asashiro-Nishi, Kumatori-cho, Sennan-gun, Osaka 590-0494 JAPAN

R. Seviour
Physics Department, Lancaster University, Lancaster, LA1 4YB, UK

M. Zisman
Lawrence Berkeley National Laboratory, 1 Cyclotron Road, Berkeley, CA 94720, US

U. Gastaldi, M. Mezzetto
Lab Nazionali di Legnaro-INFN, Via Romea, 4, I-35020 Legnaro, Padova, Italy

D. Autiero, S. Davidson
Institut de Physique Nucleaire de Lyon (IPNL), Universite Claude Bernard-Lyon I, 4, Rue Enrico Fermi, 69622 Villeurbanne Cedex, France

A. Donini, E. Fernandez-Martinez, M. Maltoni, S. Rigolin
Instituto de Fisica Teorica UAM/CSIC, Facultad de Ciencias C-XVI, Universidad Autonoma de Madrid, Cantoblanco, 28049 Madrid, Spain

D. Stratakis
University of Maryland, Dept. of Physics and Astronomy, Physics Building (Bldg. 082), College Park, MD 20742-4111, US

R. Abrams, C. Bromberg
Michigan State University, 150 Administration Building, East Lansing, Michigan 48824, US

M. Bonesini, P. Negri, S. Ragazzi
INFN Milano, Dipartimento di Fisica, G. Occhialini Piazza, Scienza 3, 20126 Milano, Italy

G. Battistoni, A. Ferrari,P. Sala
Istituto Naz. Fis. Nucleare, via Celoria 16, I-20133 Milan, Italy

T. Hart
The University of Mississippi, Department of Physics and Astronomy, 108 Lewis Hall, PO Box 1848, Oxford, Mississippi 38677-1848, US

Y. Kudenko
Inst. for Nuclear Research of Russian, Academy of Sciences, 7a, 60th October Anniversary prospect, Moscow 117312, Russia

P. Gorbounov
Institute of Theoretical and Experimental, Physics, B. Cheremushkinskaya ul. 25, RU-117218 Moscow, Russia

N. Mondal
Tata Inst. of Fundamental Research, School of Natural Sciences, Homi Bhabha Rd., Mumbai 400005, India

E. Fernandez-Martinez, M. Kachelriess
Max Planck Inst. fur Phys., Werner Heisenberg Inst. fur Phys., Fohringer Ring 6, D-80805 Munich, Germany

R. Johnstone, T. Roberts
Muons Incorporated, 552 N. Batavia Avenue, Batavia, IL 60510, US

P. Migliozzi, V. Palladino, P. Strolin
Universita di Napoli Federico II, Dipartimento di Scienze Fisiche, Complesso Universitario di Monte S. Angelo, via Cintia, I-80126 Napoli, Italy

E. Baussan
Univ. de Neuchatel, Inst. de Physique, rue A.-L. Breguet 1, CH-2000 Neuchatel, Switzerland

F. Filthaut
Natl. Inst. for Nuclear and HEP, PO Box 41882, 1009 DB Amsterdam, Netherlands

A. de Gouvea
Northwestern University, Dept. of Physics and Astronomy, 2145 Sheridan Road, Evanston, Illinois 60208-3112 US

J.E. Campagne
Laboratoire de L'accelerateur Lineaire, Centre d'Orsay, Universite de Paris-Sud XI, BP 34, Batiment 200, F-91898 Orsay cedex, FRANCE

Y. Kuno, Y. Nahashima
Osaka University, Graduate School / School of Science, 1-1 Machikaneyama-cho, Toyonaka, Osaka 560-0043, Japan Graduate School of Science, Department of Physics, Osaka University, Toyonaka, Osaka, Japan

J. Cobb, W. Lau
Particle Physics Departmenet, The Denys Wilkinson Building, Keble Road, Oxford, OX1 3RH, UK

M. Nakamura
Nagoya University, 464-01, Nagoya, Japan

F. Sergiampietri
Istituto Nazionale di Fisica Nucleare, Edificio C, Polo Fibonacci Largo B. Pontecorvo, 3 I-56127 Pisa, Italy

K. MacDonald
Princeton University, Princeton, NJ, 08544, US

G. Hanson, P. Snopok
Department of Physics and Astronomy, University of California, Riverside, CA 92521, US

K. McFarland
University of Rochester, Dept. of Physics and Astronomy, Bausch and Lomb Hall, P.O. Box 270171, 600 Wilson Boulevard, Rochester, NY 14627-0171 US

D. Meloni
Univ. delgi Studi di Roma, La Sapienza, Dipt. di Fisica G. Marconi, Piazzale Aldo Moro 2, I-00185 Rome, Italy

L. Tortora
Universita' degli Studi di "Roma Tr", Dipartimento di Fisica "Edoardo Amaldi", Istituto Nazionale di Fisica Nucleare, Via della Vasca Navale 84, 00146 Roma, Italy

C. Andreopoulos, R. Bennett, S. Brooks, R. Edgecock, D.Kelliher, S. Machida, C. Prior, G. Rees, C. Rogers, K. Tilley
STFC Rutherford Appleton Laboratory, Chilton, Didcot, Oxfordshire, OX11 0QX, UK

N. Spooner
University of Sheffield, Dept. of Physics and Astronomy, Hicks Bldg., Sheffield S3 7RH, UK

Y. Karadzhov, R. Tsenov
Department of Atomic Physics, St. Kliment Ohridski University of Sofia, 5 James Bourchier Boulevard, BG-1164 Sofia, Bulgaria

S. King
School of Physics and Astronomy, University of Southampton, Highfield, Southampton, SO17 1BJ, UK

C.K. Jung, C. McGrew
Department of Physics and Astronomy, State University of New York, Stony Brook, NY 11794-3800, USA

M. Dracos, F. Osswald
Institut de Recherches Subatomiques, 23 Rue du Loess, BP28-F67037, Strasbourg, France

H. Aihara, T. Kajita, K. Kaneyuki
Univ. of Tokyo, Dept. of Physics, 7-3-1 Hongo, Bunkyo-ku, Tokyo 113, Japan

P. Galeotti
Univ. degli Studi di Torino, Dipartimento di Fisica Teorica, Via Pietro Giuria, 1, 10125 Torino, Italy

A. Romanino
Scuola Internazionale Superiore, di Studi Avanzati, via Beirut 2-4, I-34100 Trieste, Italy

A. Cervera-Villanueva, E. Couce, J.J. Gomez-Cadenas, P. Hernandez
Instituto de Fisica Corpuscular (IFIC), Centro Mixto CSIC-UVEG, Edificio Investigacion Paterna, Apartado 22085, 46071 Valencia, Spain

P. Huber
Virginia Polytechnic Inst. and State Univ., Physics Dept., Blacksburg, VA 24061-0435

D. Kielczewska, E. Rondio, A. Zalewska
Division of Particles and Fundamental Interactions, Institute of Experimental Physics, University of Warsaw

J. Back, P. Harrison, B. Morgan,
Department of Physics, University of Warwick, Coventry, CV4 7AL, UK

J.T. Sobczyk
Institute of Theoretical Physics, University of Wroclaw, pl. M. Borna 9,50-204, Wroclaw, Poland

J. Tang, W. Winter
Fakultät fr Physik und Astronomie, Am Hubland, 97074 Würzburg, Germany

S. Menary
128 Petrie Science and Engineering Building, York University, 4700 Keele St., Toronto, Ontario, M3J 1P3, Canada

K. Satalecka
DESY Zeuthen, Inst. fur Hochenergiephysik, Platanenallee 6, D-15738 Zeuthen, Germany

A. Badertscher, A. Meregaglia, A. Rubbia
Eidgenossische Tech. Hochschule (ETH), Dept. of Physics, ETH Honggerberg, CH-8093 Zurich, Switzerland

Contents

1 Introduction

Lead author: KL

2 Physics and Performance Evaluation Group

Lead authors: AD, PH, SP, WW, OY

3 Accelerator Working Group

3.1 Overview

Lead authors: SB, YM, JP, CP

3.2 Proton driver

Lead authors: CP, J.Pasternak

3.3 Target station

Lead authors: CD, HK

3.4 Muon front end

In the muon front end we are considering improvements to the baseline configuration. Recent experimental results indicate that RF cavity peak fields may be limited in the presence of magnetic fields, and we are investigating a number of techniques to mitigate this technical risk. In addition, we are considering the optimisation of the baseline to improve the muon rate and to reduce the length of the macrobunch, which may ease requirements on kickers and the muon storage rings.

3.4.1 Baseline optimisation

We are optimising the baseline approach presented in the ISS toward specification in the cost estimate exercise of IDS-NF. We are developing a baseline which is $\sim 30\%$ shorter than the ISS case and therefore more economical, while exploring the RF-dependent performance, so that we will have a solution with good acceptance, if the RF peak gradient specification must be reduced. The candidate baseline starts with the tapered solenoid from the target (20 T to 1.5 T), where

we have alotted 18.9 m for this tapered region to be followed by a drift of 60.7 m length at a constant 1.5 T field. This is followed by a 33 m long buncher with RF that decreases in frequency from 320 MHz to 240 MHz while increasing in gradient (from cavity to cavity). This is followed by an RF rotator (42 m), which then matches into an alternating solenoid cooling channel. The buncher and rotator operate with a 1.5T focusing field.

3.4.2 Alternative Technologies

Three alternative technologies are under consideration. We are examining the possibility of moving to a low RF frequency lattice, increasing the lattice length to remove the RF cavities from magnetic fields, and operating with high pressure gas to act as an insulator for the cavities.

3.4.2.1 44/88 MHz lattice

This lattice is composed of a 30 m long decay channel in 1.8T magnetic field, followed by a rotation section, a cooling section using H_2 absorbers, and an acceleration section, all three using 44 MHz cavities operating at 2 MV/m. Another cooling and acceleration section follows using 88 MHz cavities operating at 4 MV/m. Previous simulation performed using an energy of 2 GeV for the proton driver shows that the energy spread is reduced by a factor of 2 in the rotation stage. The transverse emittance in each plane is reduced by 40% in the first cooling section and by an additional 30% in the second cooling section.

3.4.2.2 Stretched lattice

Here RF cavities are taken outside of the magnetic fields by making the lattice cell longer and introducing a modicum of shielding around the coil. While this abrogates the issue of RF cavities sitting in magnetic fields, it makes the beam optics more challenging. This necessitates the use of liquid Hydrogen absorbers in the cooling section, possibly a more challenging technology, and quite an aggressive optimisation of the beam optics. Simulations show that a reasonable performance can be achieved, close to that which can be reached by the baseline.

3.4.2.3 High Pressure RF lattice

Update to go here

3.4.3 Other Options

We are also considering a few other options, for example the use of a helical magnet or tilted solenoid that would introduce dispersion into the beam. This may allow emittance exchange, where emittance is reduced in both transverse and longitudinal phase space. In addition, we are looking at a few novel options for the cooling lattice, such as a doublet magnet structure.

3.5 Muon acceleration

3.5.1 Muon linac and RLAs

To ensure an adequate survival rate for the short-lived muons, acceleration must occur at high average gradient. The accelerator must also accommodate the phase-space volume occupied by the beam after the cooling channel. The need for large transverse and longitudinal acceptances [1] drives the design of the acceleration system to low RF frequency, e.g. 201 MHz. High-gradient, normal conducting RF cavities at these frequencies would require very high peak-power RF sources. Hence, superconducting RF (SCRF) cavities are preferred. In the acceleration scheme presented we choose a state-of-the-art SCRF gradient of 17 MV/m.

3.5.1.1 Muon RLA complex

The proposed recirculatiting-linear-accelerator (RLA) based muon accelerator complex consists of the following components:

1. A 201 MHz SCRF linac pre-accelerator that captures the large muon phase space coming from the cooling channel lattice and accelerates the muons to relativistic energies, while adiabatically decreasing the phase-space volume,;
2. A low energy RLA (RLA I) that further compresses and shapes the longitudinal and transverse phase-space, while increasing the energy to 3.6 GeV; and
3. A second stage RLA (RLA II) that further accelerates muons to 12.6 GeV.

The overall layout of the accelerator complex is shown in figure 1.

Figure 1: Layout of the accelerator complex. For compactness all components (the linac and the two RLAs) are stacked vertically; $\mu^{\pm}$ beam transfer between the accelerator components is facilitated by the vertical double chicane (see text).

3.5.1.2 Linear pre-accelerator

A single-pass linac "pre-accelerator" raises the beam energy to 0.9 GeV. This makes the muons sufficiently relativistic to facilitate further acceleration in an RLA. In addition, the longitudinal phase-space volume is adiabatically compressed in the course of acceleration [2]. The large acceptance of the pre-accelerator requires large aperture and tight focusing at its front-end. Given the large aperture, tight space constraints, moderate beam energies, and the necessity of strong focusing in both planes, we have chosen solenoidal focusing for the entire linac [1]. To achieve a manageable beam size in the linac front-end, short focusing cells are used for the first 6 cryo-modules. The beam size is adiabatically damped with acceleration. This allows the short cryo-modules to be replaced with eight intermediate-length cryo-modules and then with 11 long cryo-modules as illustrated in figure 2. The initial longitudinal acceptance of the linac is chosen to be 2.5σ, i.e. $\Delta p/p = \pm 17\%$ and RF pulse length $\Delta\phi = \pm 72^\circ$. To perform adiabatic bunching [1,3] the RF phase of the cavities is shifted by 72° at the beginning of the pre-accelerator and then gradually changed to zero by the end of the linac. In the first half of the linac, when the beam is still not completely relativistic, the offset causes synchrotron motion which allows bunch compression in both length and momentum spread, yielding $\Delta p/p = \pm 7\%$ and $\Delta\phi = \pm 29^\circ$. The synchrotron motion also suppresses the sag in acceleration for the bunch head and tail. In our tracking simulation we have assumed a particle distribution that is Gaussian in 6D phase space with the tails of the distribution truncated at 2.5σ, which corresponds to the beam acceptance. Despite the large initial energy spread, the particle tracking simulation through the linac does not predict any significant emittance growth. There is a 0.2% beam loss coming mainly from particles at the longitudinal phase space boundary. Results of the simulation are illustrated in figure 3, which shows 'snapshots of the longitudinal phase space at the beginning and at the end of the pre-accelerator.

3.5.1.3 Main acceleration system

The superconducting accelerating structure is expected to be by far the most expensive component of the accelerator complex. Therefore, maximizing the number of passes in the RLA has a significant impact on the cost-effectiveness of the overall acceleration scheme [3]. We propose to use a 4.5 pass Dogbone configuration for the RLA (figure 1Fig. 1), which has the following advantages compared to a Racetrack configuration:

- Better orbit separation at the linac ends resulting from a larger (factor of two) energy difference between two consecutive linac passes [4]; and
- A favourable optics solution for simultaneous acceleration of both μ^+ and μ in which both charge species traverse the RLA linac in the same direction while passing in the opposite directions through the mirror symmetric optics of the return 'droplet arcs [5].

The Dogbone multi-pass linac optics are shown in 4. The Dogbone RLA I simultaneously accelerates the μ^+ and μ beams from 0.244 GeV to 3.6 GeV. The injection energy into the

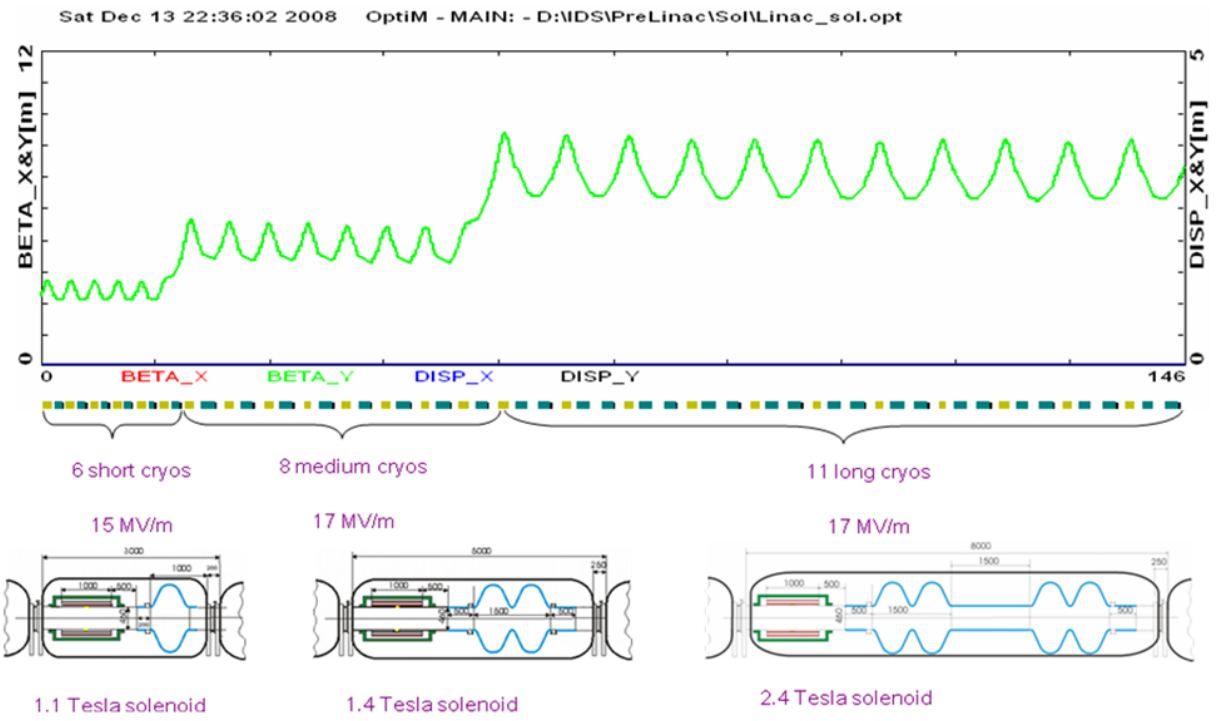

Figure 2: Top: Transverse optics of the linac - uniform periodic focusing with 6 short, 8 medium, and 11 long cryo-modules. Bottom: Layout of the short, intermediate and long cryo-modules.

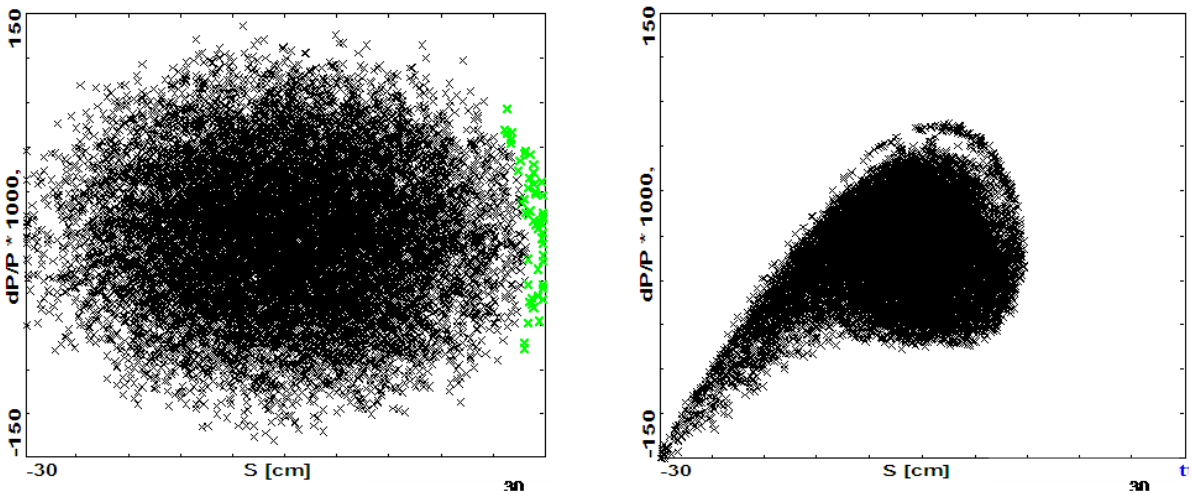

Figure 3: Particle tracking results showing adiabatic bunch compression along the linac. The longitudinal phase-space $(z, \Delta p/p)$ is shown before (left) and at the end (right) of acceleration. Particles marked in green are lost during tracking (outside the 20 cm aperture).

RLA and the energy gain per RLA linac were chosen so that a tolerable level of RF phase slippage along the linac could be maintained. We have performed a simple calculation of the phase slippage for a muon injected with initial energy E_0 and accelerated by ΔE in a linac

of length L, where the linac consists of uniformly spaced RF cavities phased for a speed-of-light particle. Our calculation used the following cavity-to-cavity iterative algorithm for the phase-energy vector:

Chris!Needhelplayingoutthisequation! (1)

where ϕ represents the phase slip of the bunch centroid at a given cavity (in degrees of 201 MHz RF), $h = L_{\mathrm{linac}}/N_{\mathrm{cav}}$, $\lambda = c/f_0$, k is the particle index, $i = 0, \ldots N_{\mathrm{cav}}1$, and V_i is the maximum accelerating voltage in cavity i. The resulting phase slippage profiles along the multi-pass RLA linacs can be summarized as follows. For the RLA injection energy of 0.9 GeV, the critical phase slippage occurs for the initial 'half-pass through the linac and it is about 40°, which is still manageable and can be mitigated by appropriate gang phase in the following linac (1-pass). For subsequent passes, the phase slippage gradually goes down and can be used, along with the sizable momentum compaction in the arcs, to compress the longitundinal phase space of the beam further. The initial bunch length and energy spread are still large at the RLA input and further compression is required in the course of the acceleration. To accomplish this, the beam is accelerated off-crest with non-zero momentum compaction (M_{56}) in the droplet arcs [3]. This induces synchrotron motion, which suppresses the longitudinal emittance growth arising from the non-linearity of the accelerating voltage. Without synchrotron motion, the minimum beam energy spread voltage over the bunch length and would be equal to $(1 - \cos\phi) \sim 9\%$ for a bunch length $\phi = 30°$. The synchrotron motion within the bunch averages the total energy gain of particles in the tail to the energy gain of particles in the core. The focusing profile along the linac of the Dogbone RLA is designed so that beams within a vast energy range can be transported within the given aperture. It is also desirable that the focusing profile is optimized to accommodate the maximum number of passes through the RLA.

In addition, to facilitate simultaneous acceleration of both μ^+ and μ^- bunches, a mirror symmetry must be imposed on the 'droplet-arc optics (oppositely charged bunches move in opposite directions through the arcs). This puts a constraint on the exit/entrance Twiss functions for two consecutive linac passes, namely $\beta^n_{\mathrm{out}} = \beta^{n+1}_{\mathrm{in}}$ and $\alpha^n_{\mathrm{out}} = \alpha^{n+1}_{\mathrm{in}}$, where $n = 0, 1, 2 \ldots$ is the pass index. Since the beam is traversing the linac in both directions throughout the course of acceleration, a 'bi-sected focusing profile [5], illustrated in 4, has been chosen for the entire linac.

At the ends of the RLA linacs, the beams need to be directed into the appropriate energy-dependent (pass-dependent) 'droplet arc for recirculation [4]. For practical reasons, horizontal rather than vertical beam separation was chosen. Rather than suppressing the horizontal dispersion created by the spreader, the horizontal dispersion has been smoothly matched to that of the outward 60° arc. Then, by an appropriate pattern of removed dipoles in three transition cells, the dispersion for the inward bending 300° arc is flipped. The droplet arc layout is shown in 5. The entire 'droplet-arc' architecture is based on 90° phase advance cells with periodic beta functions. The droplet-arc optics, which is based on FODO focusing [3], is illustrated in 5, which also shows the longitudinal phase-space occupied by the beam at the entrance and at the exit of the arc. The momentum compaction is relatively large, which guarantees significant rotation in the longitudinal phase space as the beam passes through the arc. This effect, combined

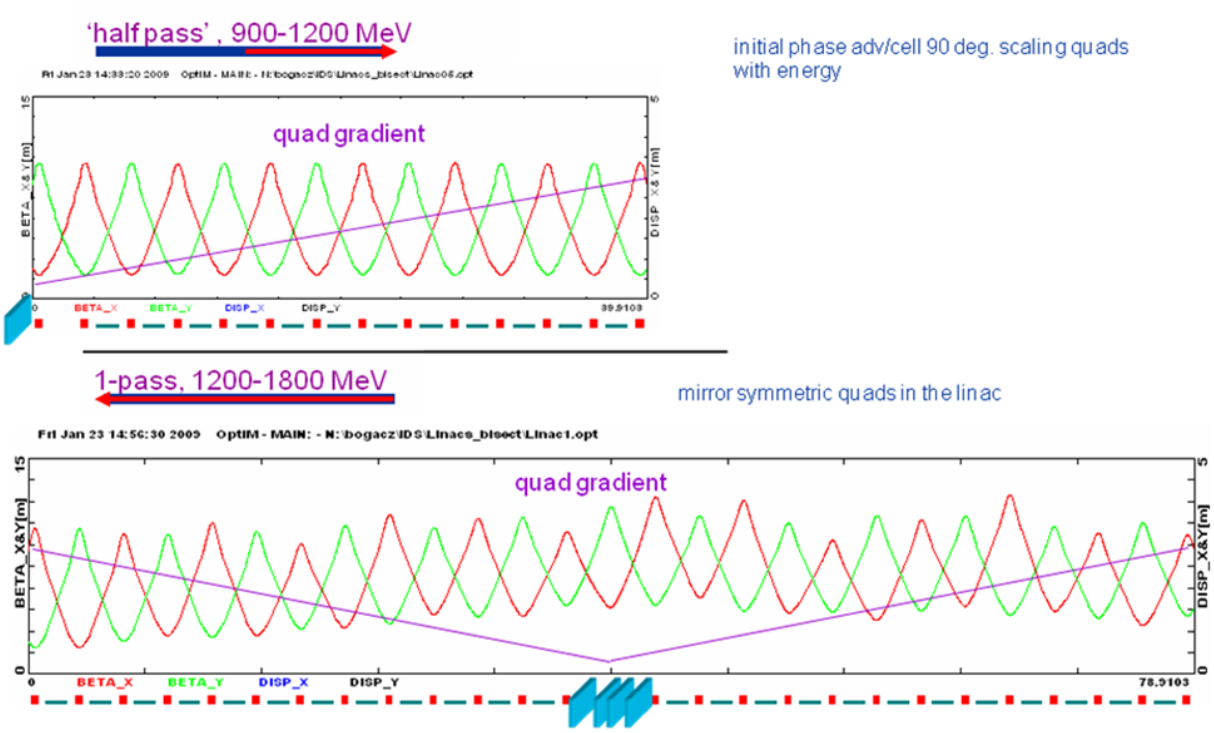

Figure 4: FODO based multi-pass linac optics. The quadrupole gradients scale up with momentum to maintain 90 phase advance per cell for the first half of the linac, then they are mirror reflected in the second half. The resulting linac optics is well balanced in terms of Twiss functions and beam envelopes; there is sufficient phase advance up to the fifth pass.

with off-crest acceleration in the subsequent linac, yields further compression of the longitudinal phase-space as the beam is accelerated.

To transfer both μ^+ and μ^- bunches from one accelerator to the other, which is located at a different vertical elevation, we use a compact double chicane [5] based on a periodic 90° phase advance cell (in FODO style). Each 'leg of the chicane involves four horizontal and two vertical bending magnets, forming a double achromat in the horizontal and vertical planes, while preserving periodicity of the beta functions.

3.5.1.4 Accelerator performance

The 6D distribution at the end of the cooling channel [5] was used to define initial longitudinal and transverse acceptances. The 6D distribution was then traced through all stages of the accelerator complex. The resulting longitudinal emittance evolution is shown in figure 5. The phase space at the RLA exit is characterized by $\Delta p/p = 0.012$ (rms) and $\Delta z = 8.5$ cm (rms). A similar end-to-end tracking study was carried out for the transverse phase space. Overall, 2% of the beam was lost out of the dynamic aperture. These losses may be mitigated by using chromaticity correcting sextupoles [4] placed at the spreader and recombiner regions of the droplet arcs.

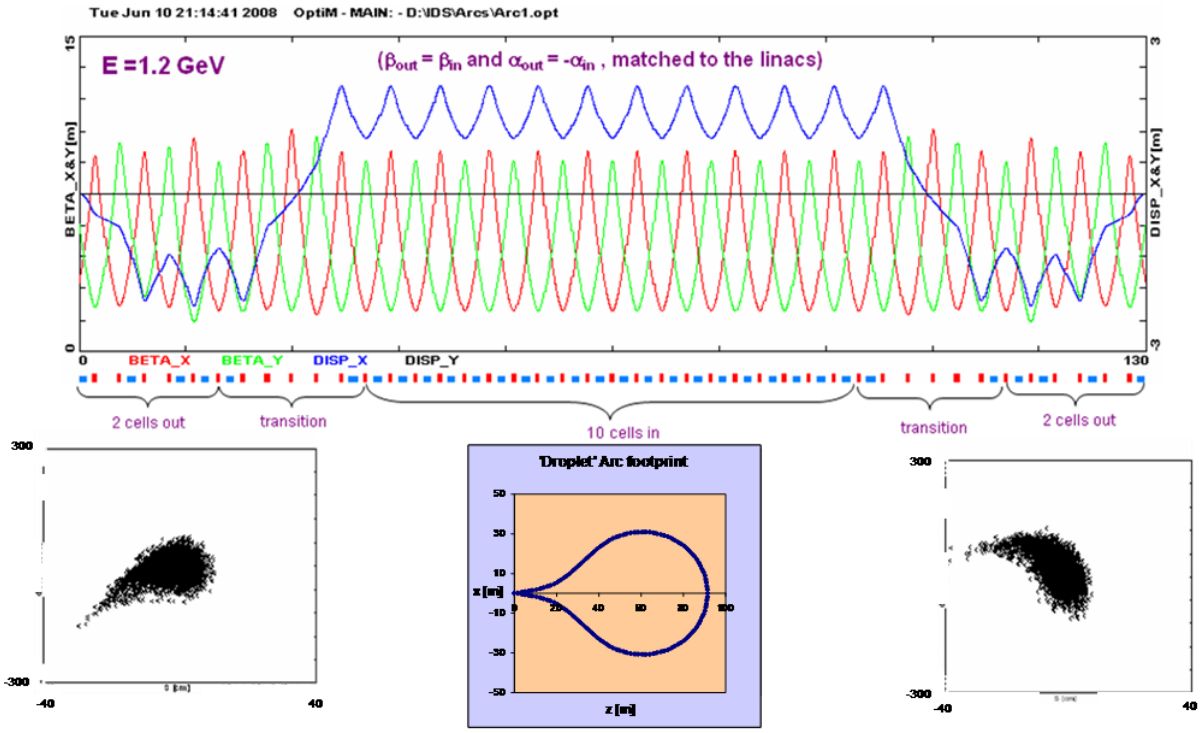

Figure 5: Top: 'Droplet arc optics, showing the uniform periodicity of beta functions and dispersion. Bottom: Particle tracking results showing the longitudinal phase-space compression. The longitudinal phase space (s [cm], $\Delta p/p \times 1000$) is shown at the beginning (left) and at the end (right) of the arc.

3.5.1.5 Linac and RLA conclusions

In summary, the results of our study suggest that there are no obvious physical or technical limitations precluding design and construction of an accelerator complex based on a pair of 4.5-pass Dogbone RLAs for acceleration of muons to 12.6 GeV. Design choices made in the proposed acceleration scheme were driven by the beam dynamics of large phase-space beams. Finally, the presented end-to-end simulation validates the efficiency and acceptance of the accelerator system.

3.6 Muon FFAG

Lead authors: SB, SM

3.7 Muon storage rings

Lead authors: MA, CP

4 Detector Working Group

4.1 Overview

Lead authors: ABr, AC, NM, PS

4.2 Software and analysis framework

Lead authors: AC, NM, PS

4.3 Magnetised Iron Neutrino Detector

Lead authors: AC, PS, AL

4.4 Totally Active Scintillator Detector

Lead authors: ABr, ME

4.5 Near detector

The main aim of the Near Detector of the Neutrino Factory is to help minimize the systematic errors associated with the oscillation measurements at the far detector. This includes precisely measuring the absolute neutrino flux as well as the relevant neutrino cross sections needed to estimate the background to oscillation measurements at the far detector.

The importance of a Near Detector to the physics program of the Neutrino Factory was emphasized most recently by the work of Tang and Winter [6]. In figure 6, the allowed $\sin^2\theta_{13}$-δ_{CP} region for a neutrino factory with one and two far detectors is illustrated. As can be seen, the impact of near detectors is very large for both the one and two detector scenarios.

A secondary goal of the Near Detector is to take advantage of the large flux of neutrinos for a dedicated study of neutrino-nucleus interactions looking for new physics and non-standard interactions. It has been pointed out [6] that near detectors could be very relevant for the extraction of neutrino source non-standard interactions since these would exhibit an unambiguous *zero-distance* effect. Because there are no tau neutrinos in the beam, Tang and Winter suggest that the most interesting option may be to use near detectors to measure ν_{tau} appearence.

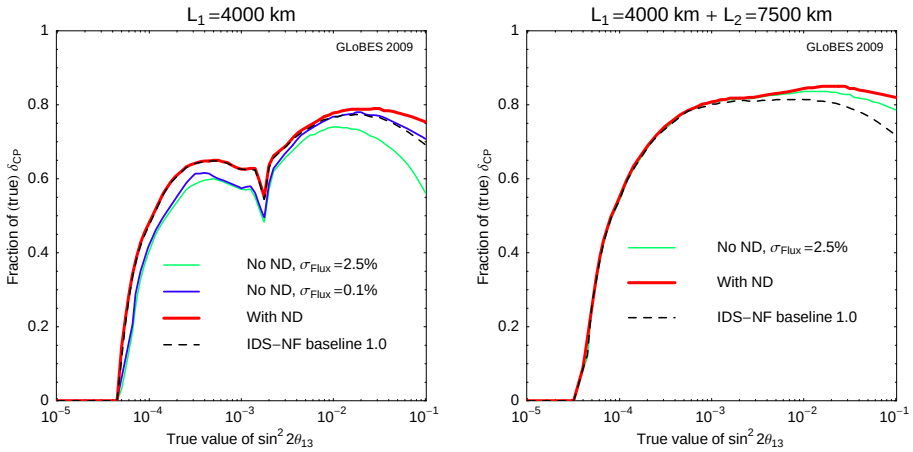

Figure 6: CP violation discovery reach as a function of true $\sin^2\theta_{13}$ and the fraction of (true) δ_{CP} for one far detector (left) and two far detectors (right) at the 3σ CL

4.6 Simulation of the neutrino beam and measurement of the neutrino flux at the Near detector

Full simulation of the neutrino beam for all neutrino flavours and including polarization states of the muon are now available [7,8]. The energy distribution of the resulting neutrino events for both ν_μ and ν_e and for both polarization states of the parent muon is shown in figure 7. The vertical dotted lines are explained in the next section.

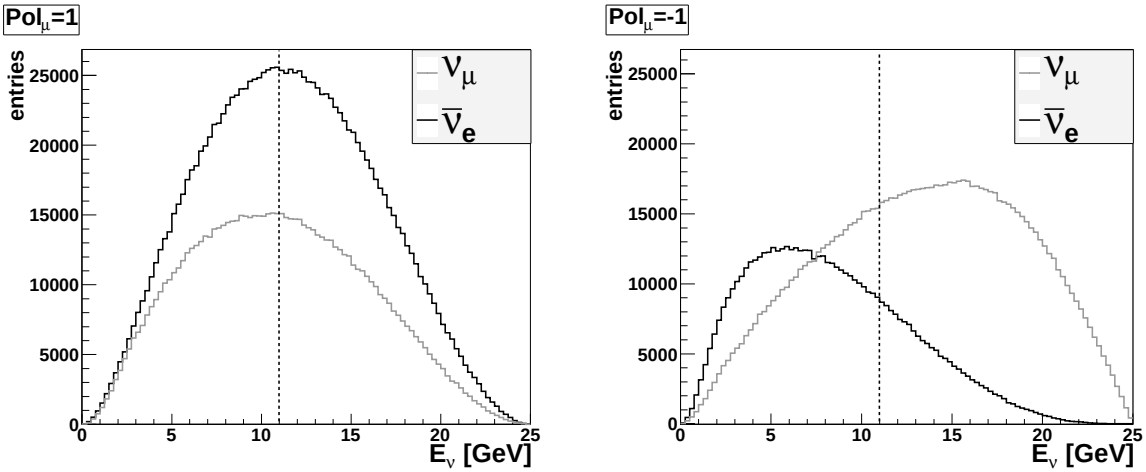

Figure 7: Distributions of the neutrino energy over a near detector of radius 1.5 m for the two polarizations of the decaying muons. Dotted lines indicate the threshold for the leptonic processes used to determine the neutrino flux.

The quasi-elastic scattering off electrons can be used to measure the flux, because its absolute cross-section can be calculated theoretically with enough confidence. The two processes of

interest for neutrinos from μ^- decays are:

$$\nu_\mu + e^- \rightarrow \nu_e + \mu^-; \tag{2}$$

and

$$\bar{\nu}_e + e^- \rightarrow \bar{\nu}_\mu + \mu^-. \tag{3}$$

Both processes have a threshold at $\sim 11\ GeV$. The energy spectra of the beam neutrinos hitting the near detector are shown in figure 7, where the threshold for the two processes of interest is shown with doted line.

If we want to measure the neutrino flux by using the quasi-elastic scattering off electrons (for earlier measurements of these processes see [9, 10]), the near detector has to be able to distinguish between the leptonic events (processes (2) and (3)) and inclusive charged-current (CC) neutrino interactions with nucleus $\nu_\mu + N \rightarrow \mu^- + X$, which are a few orders of magnitude more intensive. This implies that the near detector must be able to measure the angle between the beam axis and the direction of the outgoing muon θ_μ, the momentum of the outgoing muon, thus the energy E_μ, the transverse momentum $p_\perp$, and the total recoil (hadronic) energy E_{had}.

Different variables for suppression of the background from inclusive νN CC reactions have been examined:

- muon scattering angle θ_μ;
- transverse momentum $p_\perp$;
- $E_\mu * \theta_\mu^2$; and
- recoil (hadronic) energy E_{had}.

Spectra of the events over smeared θ_μ and $E_\mu * \theta_\mu^2$ for several resolution scenarios and for cuts on the recoil energy depicted have been performed. Examples are shown in figures 8 and 9. or a decisive choice more detailed simulation of the background with $\theta_\mu \rightarrow 0$ is needed, since it was shown earlier [11] that θ_μ is more efficient than $p_\perp$ for signal extraction.

4.7 Plans for 2010

Our plans for the year 2010 include:

- specification of detector design and size;
- full GEANT4 simulation to obtain "true" values of the measurables;
- implementation of some reconstruction and obtaining of "measured" values; and
- definition of a procedure for flux determination based on statistical subtraction of the inclusive background and estimation of expected uncertainties.

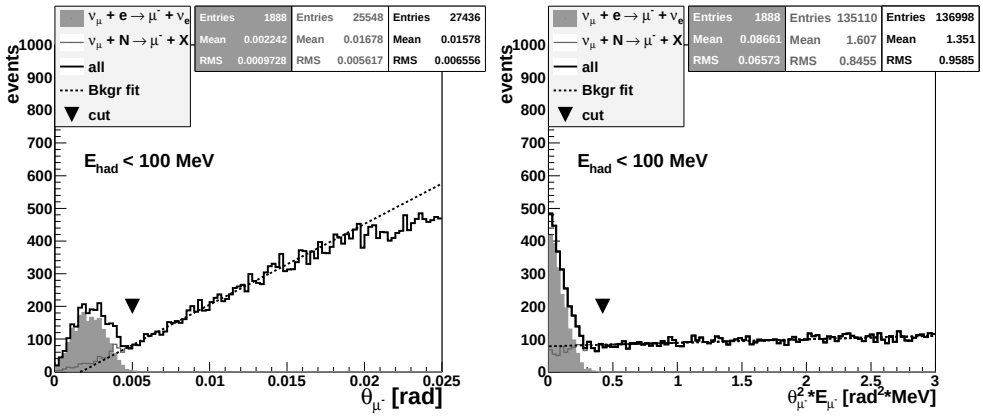

Figure 8: "Measured" distributions over the polar angle θ_μ (left) and the variable $\theta^2_\mu E$ (right) of the outgoing muons smeared with the following resolutions: $\sigma(\theta) = 0.1\ mrad$; $\frac{\sigma(E_\mu)}{E_\mu} = 1\%$; $\frac{\sigma(E_{had})}{E_{had}} = 1\%$. The leptonic events (1888 altogether) are filled with gray, the hadronic events (601 on the left panel and 838 on the right one) are plotted in gray and the total spectrum (2476 events on the left and 2725 events on the right) is in black. The cut value is denoted by black inverted triangle. Doted lines indicate the background extrapolation which gives, below the cut value, 455±53 events on the left and 1127±26 events on the right.

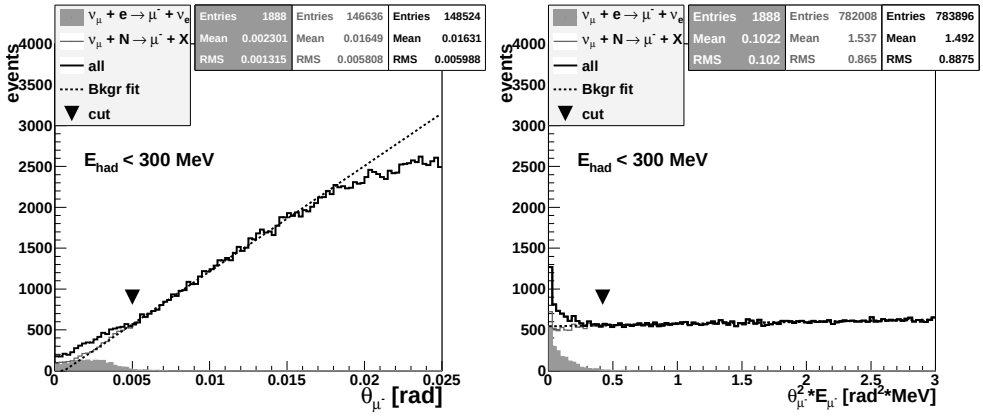

Figure 9: "Measured" distributions over the polar angle θ_μ (left) and the variable $\theta^2_\mu E$ (right) of the outgoing muons smeared with the following resolutions: $\sigma(\theta) = 1.0\ mrad$; $\frac{\sigma(E_\mu)}{E_\mu} = 10\%$; $\frac{\sigma(E_{had})}{E_{had}} = 10\%$. The leptonic events (1888 altogether) are filled with gray, the hadronic events (642 on the left panel and 893 on the right one) are plotted in gray and the total spectrum (2424 events on the left and 2726 events on the right) is in black. The cut value is denoted by black inverted triangle. Doted lines indicate the background extrapolation which gives, below the cut value, 587±64 events on the left and 1196±26 events on the right.

Acknowledgements

We would like to thank

References

[1] S. Bogacz *J. Phys. G: Nucl. Part. Phys.* **29** (2003) 1723.

[2] B. Autin *et al. J. Phys. G: Nucl. Part. Phys.* **29** (2003) 1637.

[3] J. Berg *Phys. Rev. ST Accel. Beams* **9** (2006) 011001.

[4] S. Bogacz *Nucl. Phys. B* **149** (2005) 309.

[5] S. Bogacz *Nucl. Phys. B* **155** (2006) 324.

[6] J. Tang and W. Winter, "On near detectors at a neutrino factory," *Phys. Rev.* **D80** (2009) 053001.

[7] **GENIE** Collaboration, "GENIE web site." http://www.genie-mc.org.

[8] **GENIE** Collaboration, C. Andreopoulos *et al.*, "The GENIE Neutrino Monte Carlo Generator." arXiv:0905.2517v1.

[9] **CHARM II** Collaboration, P. Vilain *et al. Phys. Lett.* **B 364** (1995) 121.

[10] S. Mishra *et al. Phys. Lett.* **B 252** (1990) 170.

[11] Y. Karadzhov. Poster No. 56 at NuFact09, Chicago, July 20-25, 2009.